Electromagnetic response of composite superconducting wires

L.J.M. van de KLUNDERT, E.M.J. NIESSEN* and P.J. ZANDBERGEN[1]
*Faculty of Applied Physics, [1]Faculty of Applied Mathematics, University of Twente, P.O. Box 217,
7500 AE Enschede, The Netherlands (*author for correspondence)*

Key words: superconductors, magnet stability, ac losses

Abstract. In this article a review is given of analytical and numerical calculations on the electromagnetic properties of composite superconducting wires. The review is based on the research performed at the University of Twente during the last ten years. Due attention is given to related results in the literature.

The basic elements of the description are the Maxwell equations supplemented with a set of constitutive equations, relating the electric field **E** and the current density **j** in the composite. The problem is non-linear due to the non-linear **E**–**j** relation describing the superconducting filaments.

The basic analytical and numerical tools for analyzing engineering problems are presented. Furthermore a synopsis is given of characteristic types of numerical results. Some comparisons between analytical and numerical results are also given.

Dedication
The first author suddenly passed away, when this paper was nearly finished. We therefore dedicate this article to the memory of Professor Louis van de Klundert, who was one of the world's leading researchers in the industrial application of superconductivity.

1. Introduction

1.1. Application of large current superconductivity

The practical use of superconductors in large electromagnets has steadily grown since the discovery of the so-called 'hard' type II superconductors, like NbTi and $NbSn_3$, in the late fifties. Already in the early sixties bubble chamber magnets with more than $10\,m^3$ free volume were constructed and used continuously for many years. Also other magnet systems like 4–6 km rings of accelerator dipoles, TEVATRON at Fermilab and HERA at DESY, have been constructed successfully and are operational. Design studies and prototypes testing for Accelerator rings of 27 km and 10 T (LHC, CERN) and 80 km at 6 T (SSC, Dallas) are underway. The first superconducting tokamak T-7 was constructed in the Kurchatov Institute in Moscow and nowadays several much larger systems, TORE SUPRA in Cadarache and T-15 in Moscow, are in operation. Still larger tokamak systems, like NET and ITER, are now under design and are intended to demonstrate the possibility of energy production by controlled fusion in the next decade.

The application of superconductors in levitated trains both for levitation and propulsion with speeds up to 512 km/hr have been demonstrated more than 10 years ago. Still under design and construction are large components for energy production and transport systems at power frequencies, 50–60 Hz. Here we can mention generators, transformers and transport lines. The advantage of using superconductors in quasi DC systems, the large ones mentioned above and small ones, e.g. MRI and laboratory magnets, is the reduction of the

power consumption by at least 6 orders of magnitude compared to conventional ones. In AC systems the large reduction in weight and size and better controllability seems to be of major importance, although the reduction in power loss is still considerable.

The average current density in superconducting systems ranges from 50–500 A/mm^2 in external fields up to 12 T. Field rates in AC systems, and in DC systems under fault conditions, may locally be in the range from 10–1000 T/s, either parallel or perpendicular to the local conductor direction. Consequently, larger demands exist on the mechanical stability of superconducting systems than in conventional ones. Moreover, under these conditions the superconducting state is often required to be maintained or the transition to the normal state (quench) has to be performed in a predictable way, such as not to damage the system.

In this paper a review will be given of the electrodynamics of superconductors based primarily on the research performed at the University of Twente during the last ten years. Of course relevant results as reported elsewhere in the literature are taken into account. The review is restricted to the analytical and numerical investigation of twisted wires. Three topics are of main interest: the current carrying capacity, the dissipation and the electromagnetically induced quench. For simplicity all calculations have been performed under isothermal conditions.

1.2. Superconductors, wires and cables

Superconducting wires generally consist of many (10^2–10^6) filaments of superconducting material embedded in a normal conducting matrix: Cu, CuNi or Al. For reasons of loss power reduction and electromagnetic stability the wire is – after drawing it down to almost the desired diameter – twisted in the last reduction step with a twist length L_p ranging from 10 to 100 times the wire radius R.

If η_{sc} is the volume fraction of superconducting material and N_f the number of filaments, the filament radius R_f is given by

$$R_f = R\sqrt{\eta_{sc}/N_f} \,. \tag{1.2.1}$$

Typical values are 0.1–50 μm for R_f, 0.1–0.5 mm for R and 0.1–0.5 for η_{sc}.

Figure 1.1 gives cross sections of some wires. It may be seen that the filament area may or may not include the centre part of the wire. The outer shell of the wire that does not contain filaments may be thick or thin. If we assume that the ring shaped filamentary zone extends from r_1 till r_2, $0 \leq r_1 < r_2 \leq R$, so occupying the fraction $\eta_f = (r_2^2 - r_1^2)/R^2$ of the total cross section, the local fraction of superconductor in the filamentary zone equals

$$\eta = \eta_{sc}/\eta_f \,. \tag{1.2.2}$$

This value of η plays an important role in the next section. In many examples in this paper, however, we will assume that the filaments are uniformly distributed over the cross section of the wire, unless a specific configuration is mentioned.

Figure 1.2 shows the cross section of superconducting cables used for accelerator dipoles and tokamaks. The contact points between the individual wires, usually called strands, will allow for closed current paths and consequently for extra loss power induced by external
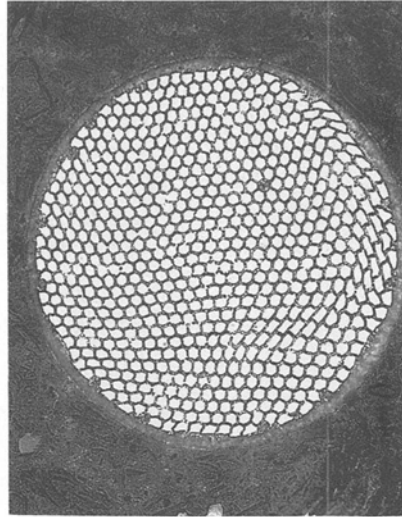
(a)
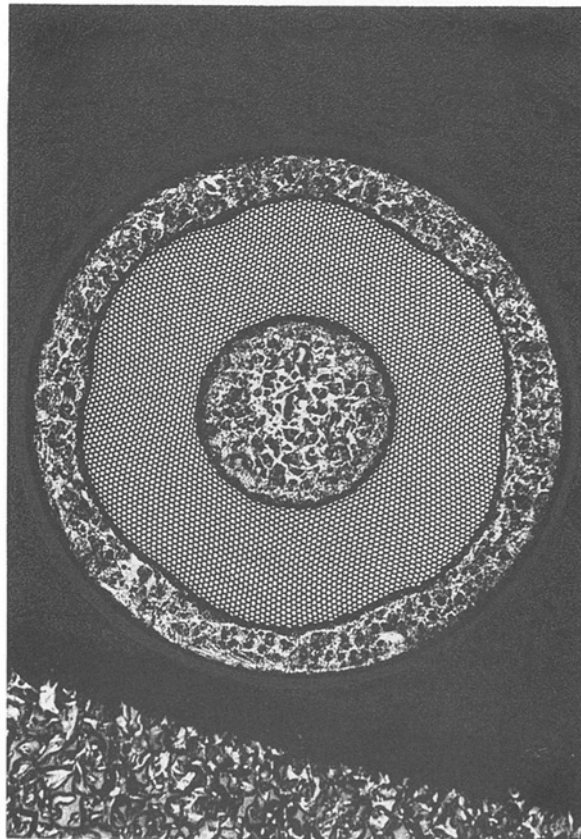
(b)

Fig. 1.1. Cross sections of some multifilamentary superconducting composite wires. The filament area may (a) or may not (b) include the centre part of the wire.
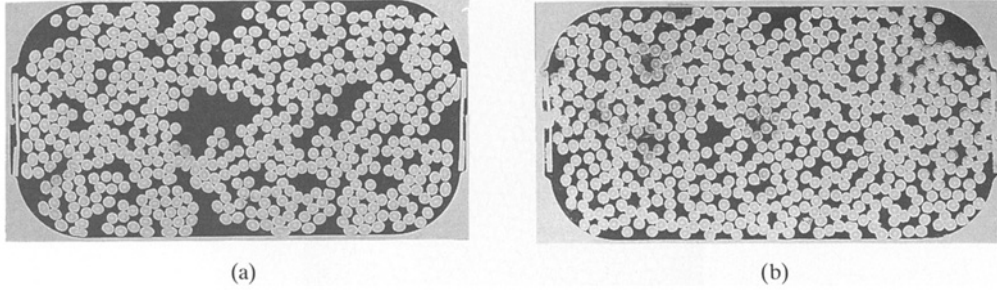
Fig. 1.2. Cross section of superconducting cables used for accelerator dipoles and tokamacs: *T*-type (a), *L*-type (b).

field changes. The *L*-type gives a much more regular distribution of the voids than the *T*-type (see Fig. 1.2).

The evaluation of the electrodynamic response in a twisted multifilamentary wire can be achieved by solving the Maxwell equations supplemented with an appropriate set of constitutive equations and boundary conditions. In earlier works also simplified potential theory has been used, whereas network approaches still find applications.

2. The mathematical formulation of the problem

2.1. The Maxwell equations

In general the Maxwell equations read:

$$\nabla \times \mathscr{E} = -\partial_t \mathscr{B} , \qquad \nabla \times \mathscr{H} = j + \partial_t \mathscr{D} , \tag{2.1.1}$$

where $\mathscr{E}$ is the electric field, $\mathscr{B}$ the magnetic field, $\mathscr{H}$ the magnetic field strength, j the current density and $\mathscr{D}$ the electric displacement [1]. Using Carr's continuum model [2] the behaviour of composite superconductors will be described in terms of averaged quantities $\mathbf{E}$, $\mathbf{B}$, $\mathbf{j}$ and the so-called magnetization $\mathbf{M}$. The Maxwell equations in a conducting non-magnetic composite and in slowly time varying fields are then given by:

$$\nabla \times \mathbf{E} = -\partial_t \mathbf{B} , \tag{2.1.2}$$

$$\nabla \times (\mathbf{B} - \mu_0 \mathbf{M}) = \mu_0 \mathbf{j} . \tag{2.1.3}$$

Since $\mathbf{M}$ results from macroscopic currents (see Section 2.5) in the filaments and varies much weaker in space and time than $\mathbf{B}$ the term $\mu_0 \mathbf{M}$ can be neglected in (2.1.3). In cylindrical coordinates we can write:

$$\frac{1}{r} \partial_\varphi E_z - \partial_z E_\varphi = -\partial_t B_r , \qquad \frac{1}{r} \partial_\varphi B_z - \partial_z B_\varphi = \mu_0 j_r ,$$

$$\partial_z E_r - \partial_r E_z = -\partial_t B_\varphi , \qquad \partial_z B_r - \partial_r B_z = \mu_0 j_\varphi , \tag{2.1.4}$$

$$\frac{1}{r} (\partial_r r E_\varphi - \partial_\varphi E_r) = -\partial_t B_z , \qquad \frac{1}{r} (\partial_r r B_\varphi - \partial_\varphi B_r) = \mu_0 j_z ,$$

and, since $\nabla \cdot (\nabla \times A) = 0$ for any vector, it may be beneficial to replace one of the above equations by:

$$\nabla \cdot \mathbf{B} = \frac{1}{r}(\partial_r r B_r + \partial_\varphi B_\varphi) + \partial_z B_z = 0 \,,$$

$$\nabla \cdot \mathbf{j} = \frac{1}{r}(\partial_r r j_r + \partial_\varphi j_\varphi) + \partial_z j_z = 0 \,. \tag{2.1.5}$$

2.2. Phenomenology of composite superconductors

Taking into account that $R_f / L_p \sim 10^{-3}$, i.e. the filaments are almost parallel to each other, it is useful to define a local coordinate system for the constitutive equations with one coordinate, $e_\parallel$, parallel to the filament direction and two, e_1 and e_2, in the plane perpendicular to $e_\parallel$. Then we have:

$$j_\parallel = \sigma_\parallel E_\parallel + \eta j_p(\mathbf{E}, \mathbf{B}, \dot{\mathbf{B}}) \,,$$

$$j_1 = \sigma_{11} E_1 + \sigma_{12} E_2 \,,$$

$$j_2 = \sigma_{12} E_1 + \sigma_{22} E_2 \,. \tag{2.2.1}$$

j_p is the superconducting current density and σ_{ij} are elements of the conductivity matrix. The coefficient $\sigma_\parallel$ is given by $\sigma_\parallel = (1 - \eta)\sigma_0$ where σ_0 is the bulk conductivity of the matrix material.

For arrangements of filaments with 3-, 4- or 6-fold rotational symmetry, the coarse grained values of the conductivity matrix reduce to

$$\sigma_{12} = 0 \quad \text{and} \quad \sigma_{11} = \sigma_{22} = \sigma_\perp \,.$$

Carr [3] states that this isotropic value $\sigma_\perp$ is given by

$$\sigma_\perp = \sigma_0(1 + \eta)/(1 - \eta) \quad \text{or} \quad \sigma_\perp = \sigma_0(1 - \eta)/(1 + \eta) \,, \tag{2.2.2}$$

whenever the filament material does or does not contribute to the transverse current conduction, respectively. This is mainly determined by the properties of the matrix superconductor interface. Usually non-conducting filaments are assumed in Cu matrix, whereas perfect conducting material is assumed, when a highly resistive CuNi matrix is used. Kanbara [4] and Rem [5] investigated the validity of relation (2.2.2). Recently it was shown [6] that for hexagonal filaments in a 6-fold symmetry the maximum deviation of the numerically calculated $\sigma_\perp$ from the value given above is about 2% at $\eta = 0.5$.

A generally accepted expression for the superconducting current density j_p does not exist and only simplified expressions, valid in some regimes can be given. The strong non-linear behaviour of the superconducting material under DC conditions can be approximated by either a power law

$$E_\parallel = E_0^{DC}(|j_p|/j_c)^n \, \text{sign}(j_p) \quad \text{or} \quad j_p = j_c \sqrt[n]{|E_\parallel|/E_0^{DC}} \cdot \text{sign}(E_\parallel) \tag{2.2.3}$$

or an exponential expression [7, 8]

$$E_\| = E_0^{DC} \frac{j_p}{j_c} \exp[(|j_p| - j_c)/j_1] \quad \text{or} \quad j_p = j_c \left[1 + (j_1/j_c) \ln\left(E_\| \Big/ \left(E_0^{DC} \frac{j_p}{j_c}\right)\right) \right] \text{sign}(E_\|) ,$$

$$(2.2.4)$$

whenever $|E_\|| < E_0^{DC}$. j_c can be referred to as the critical current density. The ratio j_1/j_c, called the smoothness factor, is typically smaller than $2 \cdot 10^{-2}$.

If we assume the usual linear critical state relation

$$E_\| = \rho_s [j_p - j_c \, \text{sign}(E_\|)] + E_0^{DC} , \quad \text{for } |E_\|| > E_0^{DC} \tag{2.2.5}$$

with ρ_s the flux flow resistivity, for larger values of $|E_\||$, a continuous function $j_p(E_\|)$ exists over the entire j_p domain. The 'critical' current density j_c is a function of $B_\perp = (B_1^2 + B_2^2)^{1/2}$ and $B_\|$ [9] and temperature T.

Under AC conditions, i.e. both $\dot{B}_\perp$ and $\dot{B}_\| \neq 0$, filaments exhibit a dynamic resistance described by the following relations

$$j_p = j_c E_\|/E_0^{AC} , \qquad |E_\|| < E_0^{AC} ,$$

$$j_p = j_c \, \text{sign}(E_\|) , \qquad |E_\|| > E_0^{AC} . \tag{2.2.6}$$

For round filaments $E_0^{AC} = (8/3\pi)R_f|\dot{B}_\perp|$ [10]. The influence of $B_\|$ on the dynamic resistance never has been investigated. Since the DC resistivity will become much smaller than the dynamic resistivity already close to j_c we will neglect the DC resistivity in all numerical AC calculations. Filaments are said to be unsaturated or saturated, whenever $|j_p|$ is smaller or equal to j_c respectively. A sharp boundary separates the unsaturated from the saturated regions in the filamentary zone.

In cylindrical coordinates the constitutive equations then read

$$j_r = \sigma_\perp E_r ,$$

$$j_\varphi = \beta r j_s + \sigma_{\varphi\varphi} E_\varphi + \sigma_{\varphi z} E_z , \tag{2.2.7}$$

$$j_z = j_s + \sigma_{\varphi z} E_\varphi + \sigma_{zz} E_z ,$$

with: $\beta = 2\pi/L_p$, $\text{tg} \, \psi = \beta r$, j_s is the superconducting component of j_z:

$$j_s = \eta j_p \cos \psi ,$$

$$\sigma_{\varphi\varphi} = \sigma_\perp \cos^2\psi + \sigma_\| \sin^2\psi = \sigma_\perp + \Delta\sigma \sin^2\psi , \qquad \sigma_{\varphi z} = \Delta\sigma \sin \psi \cos \psi , \tag{2.2.8}$$

$$\sigma_{zz} = \sigma_\| \cos^2\psi + \sigma_\perp \sin^2\psi = \sigma_\| - \Delta\sigma \sin^2\psi ,$$

where $\Delta\sigma = \sigma_\| - \sigma_\perp$.

The above model originates from Carr and is called the anisotropic continuum model.

A further simplification of the constitutive equations can be obtained by putting $E_0^{DC} = E_0^{AC} = 0$. This means that in case of AC conditions the filament radius and its resulting dynamic resistivity is neglected. This is allowed whenever the (induced) components of **E** are

much larger than E_0^{AC}. Filaments thus will be saturated whenever $E_\| = E_\varphi \sin \psi + E_z \cos \psi \neq 0$. In the unsaturated case the constitutive equations further reduce to

$$j_r = \sigma_\perp E_r ,$$

$$j_\varphi = \beta r j_s + \sigma_\perp E_\varphi , \tag{2.2.9}$$

$$j_z = j_s + \sigma_\perp E_z , \qquad E_z = -\beta r E_\varphi .$$

This reduction makes the Maxwell equations accessible for analytic considerations. It may be noted that $\sigma_\|$ disappears from the equations regardless of its value.

2.3. The applied field $\mathbf{B}^A$

Each of the components of the applied magnetic field $\mathbf{B}^A$ may be periodic functions of φ and z. We separate the total field $\mathbf{B}$ in an applied and an induced part $\mathbf{B} = \mathbf{B}^A + \mathbf{B}^I$. $\mathbf{B}^A$ then is the field generated in the volume of the conductor (wire, cable, braid) by currents outside the conductor, $\mathbf{B}^I$ is the field generated in all space by currents flowing inside the conductor. In all cases considered here no current passes through the conductor surface. If $\mathbf{B}^A = \mathbf{0}$ one speaks of a self field problem.

If we follow the path of one strand in a fully transposed cable the local applied field components will vary periodically since the direction of the strand will change compared with the general direction of the applied field. Moreover, if a multi coil system like a tokamak is considered, also other period lengths of the applied field have to be considered.

In general the applied field can be thought of as the sum of four basic components. In cylindrical coordinates the two components uniform in z are

$$\mathbf{B}_1^A = B_1(\sin \varphi, \cos \varphi, 0) , \qquad \mathbf{B}_2^A = B_2(0, 0, 1)$$

and the two periodic in z:

$$\mathbf{B}_3^A = B_2\left(I_1'(pr) \sin \varphi \sin pz, \frac{I_1(pr)}{pr} \cos \varphi \sin pz, I_1(pr) \sin \varphi \cos pz \right) ,$$

$$\tag{2.3.1}$$

$$\mathbf{B}_4^A = B_4(I_1(pr) \sin pz, 0, I_0(pr) \cos pz) .$$

$\mathbf{B}_1^A$ and $\mathbf{B}_3^A$ have their main contribution in the y-direction, $\mathbf{B}_2^A$ and $\mathbf{B}_4^A$ in the z-direction. I_0 and I_1 are Bessel functions of the second kind. $p = 2\pi/L_z$, L_z is the period length in the z-direction. These four components all are regular solutions of $\nabla \cdot \mathbf{B}^A = \nabla \times \mathbf{B}^A = 0$ for $0 \leq r \leq R$.

The coefficients B_i, $i = 1, 4$, are functions of time. Two cases are considered here: the periodic time dependence $B_i = B_0 e^{-i\omega t}$ and the linear time dependence $B_0 = 0$ for $t < 0$, $B_0 = \alpha t$ for $t \geq 0$. In the latter case we have to deal with an in time decaying effect of the transient occurring at $t = 0$. For large times compared to specific response times of the system, $\dot{\mathbf{B}}^I$ will vanish and we will refer to this situation as the stationary case.

2.4. The induced field $\mathbf{B}^I$ and the boundary conditions

The shape of the induced field $\mathbf{B}^I$ outside the wire, resulting from the current distribution induced in the wire by the applied field $\mathbf{B}^A$ and the transport current I^A in general has a very

complicated structure. When the applied magnetic field is described using some Fourier terms in the φ and z-direction, higher Fourier modes can appear in the induced field outside the wire due to:

a. The non-linear $j_\parallel(E_\parallel)$ relation, which may result in the occurrence of boundaries $r(\varphi, z, t)$, separating saturated and unsaturated regions;

b. the finite sample length, due to boundary conditions at the ends, i.e. at $z = \pm L$, where $2L$ is the length of the sample.

The induced field can be calculated from $\nabla \cdot \mathbf{B}^I = \nabla \times \mathbf{B}^I = 0$ under the condition $\mathbf{B}^I(r \to \infty) = \mathbf{0}$.

For each of the applied fields $\mathbf{B}_i^A$ given in (2.3.1) we get

$$\mathbf{B}_1^I = \sum_m a_m(\sin m\varphi, \cos m\varphi, 0) \ ,$$

$$\mathbf{B}_2^I = \mathbf{0} \ ,$$

$$\mathbf{B}_3^I = \sum_n \sum_m b_{nm}(K_m'(npr) \sin m\varphi \sin npz \ , \tag{2.4.1}$$

$$K_m(npr) \sin m\varphi \sin npz/npr, \ K_m(npr) \sin m\varphi \cos npz) \ ,$$

$$\mathbf{B}_4^I = \sum_n c_n(K_1(npr) \sin npz, 0, -K_0(npr) \cos npz) \ .$$

Here a_m, b_{nm} and c_n are functions of t which still must be calculated; K_0 and K_1 are Bessel functions of the second kind.

The induced field from the transport current I^A is given by:

$$B_\varphi^I = \mu_0 I^A / 2\pi r \ . \tag{2.4.2}$$

In general the (double) summations have to be taken over an infinite number of terms. Notice that the exact form of the applied field is given, equation (2.3.1), but only the shape of the induced field outside the wire is given, equation (2.4.1). The currents and field components inside the wire must now be calculated using that the values of the coefficients in (2.4.1) follow from the continuity of $\mathbf{B}^I$ at $r = R$. In numerical calculations it is sufficient to impose the boundary conditions in an integral way [5] (see Section 4.2.2). Other boundary conditions, to be fulfilled when determining the solution of the Maxwell equations, are $E_r(R) = 0$ and $B_r^I(0) = B_\varphi^I(0) = 0$.

It may be noted that the response to a linear combination of B_i^A given in (2.3.1) is not necessarily a linear combination of B_i^I given in (2.4.1). Such complex problems, however, have not been studied so far.

2.5. The magnetization and dissipated power density

In a virgin filament, changes of the external field will induce screening currents which hold up the penetration of the external field into the filament. Flux penetration occurs because the current density is limited by the critical current density. The penetration field is the magnetic field amplitude beyond which the interior of the superconductor can no longer by shielded from the external magnetic field. As a consequence, for magnetic field changes larger than the penetration field, the total amount of superconducting material is positively or negatively

saturated. The flux penetration process is not reversible, i.e. the magnetization shows a hysteresis behaviour. Subjecting a superconductor to an alternating magnetic field therefore involves dissipation. So inside the filament a closed current loop appears having an effective magnetic moment. The averaged **M** in a multifilamentory superconductor results from adding all the small magnetic moments of current distributions inside the filaments.

We already saw this in Carr's continuum model where for averaged quantities we found equation (2.1.3). In this equation only **M** is reminiscent of the variations in current density within the filaments.

The induced screening currents will penetrate the whole filament if the field change amounts [11]

$$B_{p\|} = \mu_0 j_{c\varphi} R_f , \quad \text{in parallel field change,}$$

$$B_{p\perp} = \frac{2}{\pi} \mu_0 j_{cz} R_f , \quad \text{in perpendicular field change.} \tag{2.5.1}$$

$j_{c\varphi}$ and j_{cz} may have different values due to the production process of the wire. A field change of $2B_p$ is needed to bring the filament from one state of saturation into the opposite one. In an array of widely spaced filaments with 6-fold symmetry and a perpendicular field change larger than $2B_p$ a constant magnetization is obtained

$$M_\perp = -\frac{4}{3\pi} \eta j_{cz} R_f \, \text{sign}(\dot{B}_\perp) , \quad \text{if } \dot{B}_\| = 0 ,$$

$$M_\| = -\frac{1}{3} \eta j_{c\varphi} R_f \, \text{sign}(\dot{B}_\|) , \quad \text{if } \dot{B}_\perp = 0 . \tag{2.5.2}$$

If the filament carries a transport current equivalent to an average current density j_p the magnetization is in a good approximation reduced by a factor $1 - (j_p/j_c)^2$ [5]. The local loss power density p is given by

$$p = \mathbf{j} \cdot \mathbf{E} - \mathbf{M} \cdot \dot{\mathbf{B}}$$

$$= \sigma_\perp (E_r^2 + E_\perp^2) + \sigma_\| E_\|^2 + \eta j_p E_\| - M_\perp \dot{B}_\perp - M_\| \dot{B}_\| , \tag{2.5.3}$$

where either $\dot{B}_\perp$ or $\dot{B}_\| = 0$.

Values for $M_\perp$ and $B_{p\perp}$ for hollow filaments and filaments of square cross section have been reported by [12] and [10], respectively.

Notice that in the Maxwell equations (2.1.4) the magnetization **M** is neglected while in the loss calculations, equation (2.5.3), the loss term due to the magnetization is present. The reason for neglecting **M** in equation (2.1.4) is twofold:

1) $|\nabla \times \mu_0 \mathbf{M}| \ll |\nabla \times \mathbf{B}|$,
2) $\nabla \times \mathbf{M} = 0$ because **M** is constant if $B > 2B_p$.

3. Analytical solutions

The solution of the Maxwell equations can be found analytically only if a considerable reduction in the complexity of the problem can be obtained. Four examples will be given

below. In the first one the conductor, e.g. a hollow wire of twisted filaments, is represented by a surface current, with linear properties, only. It should be remarked that this model is also valid for a hollow cable of twisted strands. In the second and third example the solution for uniform fields perpendicular and parallel to the wire are given. In the last example the solution in one turn of a cylindrical coil placed in a uniform field perpendicular to the coil axis is presented.

The non-linear character of the problem, resulting from the non-linear $j_\parallel$-component of the constitutive equation, can be removed by assuming that the whole interior of the wire is unsaturated. In order to account for the boundary condition $E_r(R) = 0$ or $B_\varphi(R) = B_\varphi^0$ in rotational symmetric problems a surface current $\mathbf{J}$, which also behaves linearly, is introduced. $\mathbf{J}$ flows in the filament direction and has components J_z and J_φ, with $J_\varphi = \beta R J_z$. If $E_r(R^-) \neq 0$ the condition $E_r(R^+) = 0$ is fulfilled if

$$\partial_z J_z + R^{-1}\partial_\varphi J_\varphi = \sigma_r E_r(R^-), \tag{3.1}$$

which relation follows from conservation of current at the surface of the wire. $E_r(R^-)$ and $E_r(R^+)$ denote the limiting values for $r \to R$, if $r < R$ or $r > R$ respectively. The continuity of $\mathbf{B}^I$ at $r = R$ is maintained, but for B_φ^I and B_z^I the following relations replace the continuity requirement in absence of the surface current $\mathbf{J}$:

$$B_\varphi^I(R^+) - B_\varphi^I(R^-) = \mu_0 J_z, \qquad B_z^I(R^-) - B_z^I(R^+) = \mu_0 J_\varphi. \tag{3.2}$$

These discontinuity relations follow from the Stokes versions of the Maxwell equations. The analytical approximations should be compared to numerical solutions taking into account the spatial extension of the shielding currents at the surface and the non-linear $\mathbf{E}$–$\mathbf{j}$ relation. Numerical solutions will be presented in Section 4.

3.1. A hollow cylinder in a periodically applied field

If we consider a hollow cylinder of infinitesimal thickness and surface conductivity σ perpendicular to the filament direction, we can write for the most general applied field $\mathbf{B}^A$ with a fixed frequency ω [10]:

$$\mathbf{B}^A = \sum_n \sum_m a_{nm}^A \, e^{i(m\varphi + npz - \omega t)}(I_m'(npr), iI_m(npr)/npr, iI_m(npr)).$$

For $r < R$ the induced field $\mathbf{B}^I$ can be written

$$\mathbf{B}^I = \sum_n \sum_m a_{nm} \, e^{i(m\varphi + npz - \omega t)}(I_m'(npr), iI_m(npr)/npr, iI_m(npr))$$

and for $r > R$, since B_r is continuous

$$\mathbf{B}^I = \sum_n \sum_m a_{nm} \, e^{i(m\varphi + npz - \omega t)}I_m'(npR)/K_m'(npR)$$

$$(K_m'(npr), iK_m(npr)/npr, iK_m(npr)).$$

If we apply equation (3.2) we find

$$\mu_0(J_\varphi, J_z) = \sum_n \sum_m ia_{nm} \, e^{i(m\varphi + npz - \omega t)}/npR \cdot K'_m(npR)(-1, m/npr).$$

If we now write the constitutive equations in the form

$$\sigma E_\varphi = \cos^2\psi J_\varphi - \sin\psi\cos\psi J_z \,,$$

$$\sigma E_z = \sin^2\psi J_z - \sin\psi\cos\psi J_\varphi \,,$$

we find from $R^{-1}\partial_\varphi E_z - \partial_z E_\varphi = -\partial_t B_r$

$$a_{nm} = \frac{-i\mu_0\omega\sigma R(npr)^2 K'_m(npR)I'_m(npr)a_{nm}^A}{(m\sin\psi + npR\cos\psi)^2 + i\omega\mu_0\sigma R(npR)^2 K'_m(npR)I'_m(npR)}$$

and for the Ohmic loss P per unit cylinder surface

$$P = \sum_{n,m} P_{nm} = \sum_n \sum_m \frac{1}{8\sigma} \left(\frac{m\sin\psi + npR\cos\psi}{\mu_0(npR)^2 K'_m(npR)} \right)^2 |a_{nm}|^2 \,.$$

In Fig. 3.1 $P_{4,1}/P_0$ is shown for various values of $\omega\tau = \omega\mu_0\sigma R/(2\sin^2\psi)$, P_0 is the loss in a uniform steadily increasing perpendicular field $\dot{B}_x = \alpha t$:

$$P_0 = \frac{\sigma}{8\pi^2} (L_p \dot{B}_x^A)^2 (1 + \beta^2 R^2) = \frac{\sigma}{2} \dot{B}_x^{A2}(R^2 + \beta^{-2}).$$

The limit of $P_{4,1}/P_0$ for $L_z/L_p \to \infty$ equals $1/2$ because of the time averaging.

3.2. Twisted wire in uniform perpendicular field

In analogy with the previous treatment the case of a perpendicular applied field can be given. For reasons of brevity only the case of z-invariant sinusoidal time dependence of the applied field will be presented. For more details see [13], [14] and [15].
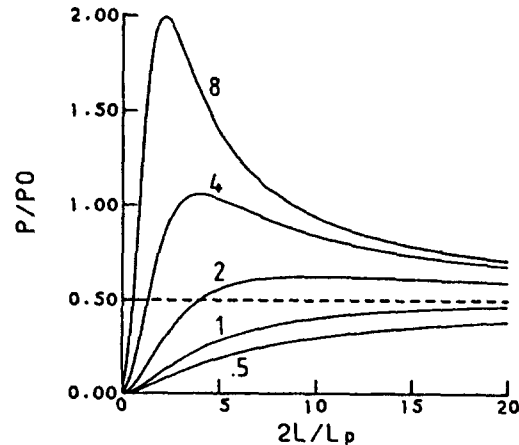

Fig. 3.1. $P_{4,1}/P_0$ for various values of $\omega\tau$ [10].

The Maxwell equations for this special case read

$$\partial_\varphi E_z = \mathrm{i}\omega r B_r \,,$$

$$-\partial_r E_z = \mathrm{i}\omega B_\varphi \,,$$

$$\partial_r r E_\varphi - \partial_\varphi E_r = \mathrm{i}\omega r B_z \,,$$

$$\partial_\varphi B_z = \mu_0 \sigma_r r E_r \,,$$

$$-\partial_r B_z = \beta r \mu_0 j_s + \mu_0 \sigma_\perp E_\varphi \,,$$

$$\partial_r r B_\varphi - \partial_\varphi B_r = r(\mu_0 j_s + \mu_0 \sigma_\perp E_z) \,.$$

(3.2.1)

Assuming

$$B_r = g \sin\varphi\, \mathrm{e}^{-\mathrm{i}\omega t} \,,$$

$$E_r = \frac{\mathrm{i}\omega}{\beta} h \sin\varphi\, \mathrm{e}^{-\mathrm{i}\omega t} \,,$$

$$\mu_0 j_s = \mathrm{i}\omega\tau k \cos\varphi\, \mathrm{e}^{-\mathrm{i}\omega t} \,,$$

with $\tau = \mu_0 \sigma_\perp / \beta^2$, we get for the surface current

$$\mu_0 J_z = -\mathrm{i}\omega\tau h(R) \cos\varphi\, \mathrm{e}^{-\mathrm{i}\omega t}$$

and $J_\varphi = \beta R J_z$, and the remaining components of E and B

$$E_\varphi = \frac{\mathrm{i}\omega}{\beta} g \cos\varphi\, \mathrm{e}^{-\mathrm{i}\omega t} \,,$$

$$B_z = -\mathrm{i}\omega\tau\beta r h \cos\varphi\, \mathrm{e}^{-\mathrm{i}\omega t} \,,$$

(3.2.2)

$$B_\varphi = \partial_r(rg) \cos\varphi\, \mathrm{e}^{-\mathrm{i}\omega t} \,.$$

Putting

$$g = A \sum_{n=0} a_n u^{2n} \,, \qquad h = A \sum_{n=0} b_n u^{2n} \,, \quad \text{with } u = \beta r$$

(3.2.3)

recurrence relations for a_n and b_n can be derived.

$$a_{-1} = b_{-1} = 0 \,, \qquad a_0 = b_0 = 1 \,,$$

$$4n(n+1)(1 - \mathrm{i}\omega\tau)a_n = \mathrm{i}\omega\tau[((2n+1)^2 - 1 + \mathrm{i}\omega\tau)b_{n-1} - (2n+1)a_{n-1}] \,,$$

$$4n(n+1)(1 - \mathrm{i}\omega\tau)b_n = \mathrm{i}\omega\tau[\mathrm{i}\omega\tau(2n+1)b_{n-1} - a_{n-1}] \,.$$

Notice that the convergence interval of the power series is bounded. From the boundary conditions A can be determined to be

$$A = 2B_0/[A + (1 - i\omega\tau(1 + \beta^2 R^2))A] ,$$ (3.2.4)

and consequently the power loss per unit length

$$S = \frac{\pi R}{2\mu_0} E_z B_\varphi^* .$$

Here B_φ^* is the complex conjugate of B_φ. If we write

$$S = \frac{\pi R^2}{2\mu_0} i\omega B_0^2(\mu' + i\mu'')$$ (3.2.5)

the values of μ' and μ'' can be plotted as shown in Fig. 3.2 [15].

For small β the $\mu''(\mu')$ curve has an ellipse as a limiting envelope whereas for $\beta \to \infty$, where the filaments degenerate in rings, the relation for a solid copper wire

$$\mu = 1 + J_2(kr)/J_0(kr) ,$$ (3.2.6)

where $k^2 = i\omega\mu_0\sigma_\perp$ and J_0 and J_2 are Bessel functions of the first kind, must be obtained. This limit cannot be verified using these series expansions for convergence reasons.

It may be noted that for small ω the power loss is [15]

$$P = \frac{\omega B_0^2}{\mu_0} \frac{\omega\tau'}{1 + (\omega\tau')^2} , \quad \text{with } \tau' = \frac{\mu_0\sigma_\perp}{2} \left[\left(\frac{L_p}{2\pi}\right)^2 + R^2 \right]$$ (3.2.7)

rather than the widely used expression for τ' where the term R^2 is omitted.
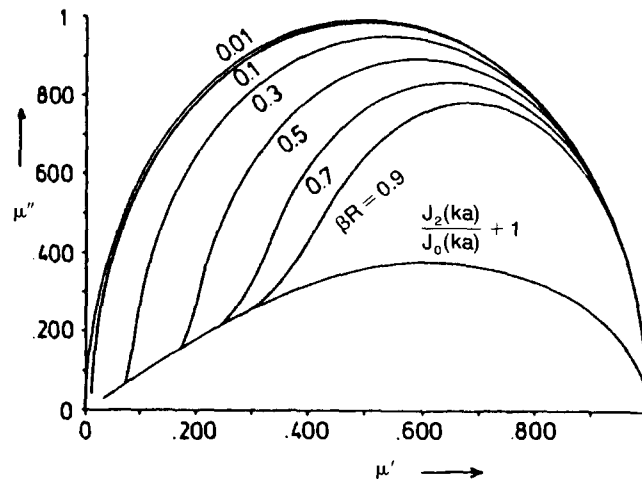

Fig. 3.2. Representation of the Poynting vector in terms of a complex permeability for a uniform perpendicular applied field [15].

3.3. Twisted wire in parallel field

The shape of the applied field is chosen to be rotational symmetric. Then the Maxwell equations read

$$-\partial_z E_\varphi = -\partial_t B_r \,,$$

$$\partial_z E_r - \partial_r E_z = -\partial_t B_\varphi \,,$$

$$\partial_r(rE_\varphi) = -r\partial_t B_z \,,$$

$$-\partial_z B_\varphi = \mu_0 \sigma_r E_r \,,$$

$$\partial_z B_r - \partial_r B_z = \beta r \mu_0 j_s + \mu_0 \sigma_\perp E_\varphi \,,$$

$$\partial_r(rB_\varphi) = r(\mu_0 j_s + \mu_0 \sigma_\perp E_z) \,.$$

(3.3.1)

If we assume that the problem is also z-invariant, we immediately get $E_r = B_r = 0$ irrespective of the time dependence of $\mathbf{B}^A$. Moreover, it can be shown that $E_z + \beta rE_\varphi = 0$ implies $B_\varphi - \beta rB_z = 0$ [16]. $E_r = 0$ implies that no current exchange in the r-direction occurs, irrespective of the value of σ_r [17, 18].

Two cases can be considered with respect to the time dependence:

$$B_z^A = 0 \quad t < 0, \qquad B_z^A = \alpha t \quad t \geq 0 \quad \text{or} \quad B_z^A = B_0\,\mathrm{e}^{-i\omega t} \,.$$

For E_φ a partial differential equation can be obtained,

$$\partial_r \frac{1}{r}(1 + \beta^2 r^2)\partial_r rE_\varphi = (1 + \beta^2 r^2)\mu_0 \sigma_\perp \dot{E}_\varphi \,.$$

(3.3.2)

In principle the equation can be solved applying a separation of variables technique. This has so far not been done. In the stationary case, i.e. after the decay of the transient effect, the solution reads

$$E_\varphi = -\alpha \ln(1 + \beta^2 r^2)/2\beta^2 r \,,$$

$$B_\varphi = \beta r\alpha t/(1 + \beta^2 r^2) \,,$$

$$B_z = \alpha t/(1 + \beta^2 r^2) \,,$$

(3.3.3)

and

$$\mu_0 j_s = 2\beta\alpha t/(1 + \beta^2 r^2)^2 \,,$$

(3.3.4)

From (3.3.2) it can be seen, that if $\sigma_\perp = 0$ ($\tau = 0$) saturation occurs first at $r = 0$ and

$$B_z^A = \alpha t = \mu_0 \eta j_c L_p/4\pi \,.$$

(3.3.5)

Thus saturation in the inner region occurs after a change in B_z^A independent of the rate of change of B_z^A.

In case a sinusoidal time dependence of B_z^A is assumed $B_z^A = B_0 e^{-i\omega t}$ it is useful to put

$$E_\varphi = i\omega g , \qquad E_z = -i\omega\beta rg ,$$

$$B_\varphi = \beta \partial_r(rg) , \qquad B_z = \frac{1}{r} \partial_r(rg) , \qquad \mu_0 j_s = k .$$

(3.3.6)

Writing

$$g = A \sum_{n=0} a_n u^{2n+1} , \qquad k = A \sum_{n=0} b_n u^{2n} , \quad \text{with } u = \beta r$$

the following recurrence relations for a_n and b_n exist:

$$a_{-1} = b_{-1} = 0 , \quad a_0 = 1 ,$$

$$4(n+1)(n+2)a_{n+1} = -[4(n+1)^2 a_n + i\omega\tau(a_n + a_{n-1})] ,$$

$$b_n = \beta^2[(2n+1)^2 a_n + i\omega\tau a_{n-1}] ,$$

$$\tau = \mu_0 \sigma_\perp / \beta^2 .$$

The constant A follows from the boundary condition for $B_\varphi^A = 0$

$$A = B_0/\beta(1 + \beta^2 R^2) \sum_{n=0} (2n+2)a_n(\beta R)^{2n} .$$

(3.3.7)

The loss power per unit of length can be determined from the real part of the Poynting vector

$$S = \frac{\pi R}{\mu_0} E \times B^* .$$

(3.3.8)

If we write

$$S = \frac{\pi R^2}{2\mu_0} i\omega B_0^2(\mu' + i\mu'')$$

the real and imaginary part of $\mu = \mu' + \mu''$ can be plotted for $\omega\tau$ and βR as a parameter. Figure 3.3 shows these curves [15]. For $\beta R = 0$, i.e. no twist, the curve for a pure metallic bar is found whereas for $\beta R \to \infty$, i.e. the filaments degenerate in rings, the semicircle of a paramagnetic material must be obtained.

3.4. Field in the plane of a turn of a cylindrical coil

In important practical applications wires are used in ring-shaped configurations, e.g. the D-coils in the Next European Torus fusion reactor [19]. In this subsection the properties of a
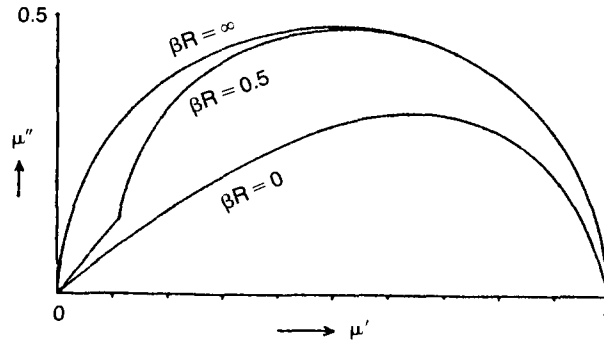
Fig. 3.3. Representation of the Poynting vector in terms of a complex permeability for a uniform parallel applied field [15].

D-coil in an AC magnetic field are studied, using an ideal torus configuration for the wire, which represents one turn of the coil. The radius of the wire is R and the mean radius of the torus is $R_0 \gg R$ (see Fig. 3.4).

The applied time dependent magnetic field is considered to be uniform and parallel to the plane of the torus with constant time derivative $\dot{B}^A$. This field, chosen in the z-direction $(\dot{B}_z^A)$ will be perpendicular to the wire for coordinates $(x, z) = (0, \pm R_0)$ and parallel for $(x, z) = (\pm R_0, 0)$. For other coordinates (x, z) on the wire the field is partly perpendicular and partly parallel.

We want to perform the calculations in the natural r, φ, θ system where θ represents the angle on the torus with the positive x-axis and r and φ are the cylindrical coordinates perpendicular to θ. The configuration and definitions are outlined in Fig. 3.4. The (r, φ, θ) system is a positive oriented orthogonal coordinate system. The coordinate transformation for the vector x with x, y and z coordinates to the new coordinate system reads:
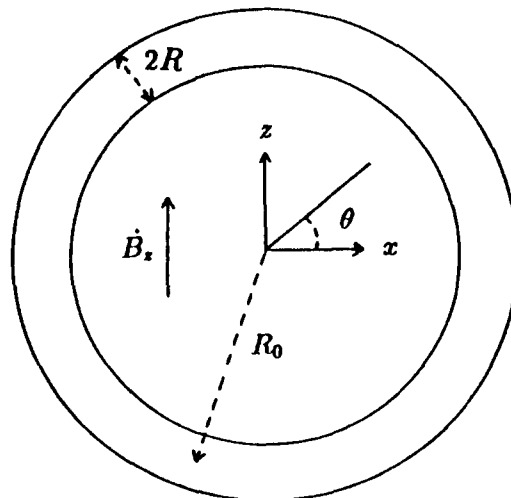

Fig. 3.4. Circular configuration for the wire with radius R in a torus shape with mean radius R_0. Here $R \ll R_0$ [20].

$$(x, y, z) = ((R_0 + r \cos \varphi) \cos \theta, r \sin \varphi, (R_0 + r \cos \varphi) \sin \theta) , \tag{3.4.1}$$

which gives for the elementary lengths:

$$h_r = 1 , \qquad h_\varphi = r , \qquad h_\theta = R_0 + r \cos \varphi . \tag{3.4.2}$$

In this new coordinate system the Maxwell equations in case of a stationary problem read:

$$(\nabla \times \mathbf{E})_r = \frac{1}{r} \partial_\varphi E_\theta - \frac{1}{R_0 + r \cos \varphi} [\partial_\theta E_\varphi + \sin \varphi E_\theta] = -\dot{B}_r^A , \tag{3.4.3}$$

$$(\nabla \times \mathbf{E})_\varphi = -\partial_r E_\theta - \frac{1}{R_0 + r \cos \varphi} [-\partial_\theta E_r + \cos \varphi E_\theta] = -\dot{B}_\varphi^A , \tag{3.4.4}$$

$$(\nabla \times \mathbf{E})_\theta = \frac{1}{r} [\partial_r (r E_\varphi) - \partial_\varphi E_r] = -\dot{B}_\theta^A . \tag{3.4.5}$$

The applied magnetic field $\dot{B}_z^A$ can be written in its r, φ, θ components: $\dot{\mathbf{B}}^A = \dot{B}_z^A (\cos \varphi \sin \theta, -\sin \varphi \sin \theta, \cos \theta)$. Conservation of the bulk current density $\mathbf{j}$ in the interior of the wire is written as:

$$\nabla \cdot \mathbf{j} = \frac{1}{r} [\partial_r (r j_r) + \partial_\varphi j_\varphi] + \frac{1}{R_0 + r \cos \varphi} [\cos \varphi j_r - \sin \varphi j_\varphi + \partial_\theta j_\theta] = 0 . \tag{3.4.6}$$

At the surface of the wire $r = R$ we consider a surface current with components J_φ and J_θ in the φ and θ direction respectively. From the fact that no current flows out of the wire at the boundary $r = R$, conservation of current is written as:

$$-(R_0 + R \cos \varphi) R j_r (r = R) + (R_0 + R \cos \varphi) \partial_\varphi J_\varphi - J_\varphi R \sin \varphi + R \partial_\theta j_\theta = 0 . \tag{3.4.7}$$

The differential equations cannot be solved directly so we use a power series in r because $R \ll R_0$. We show the calculation of E_φ in detail. Substituting $E_\parallel = 0$ so $E_\theta = -\beta r E_\varphi$ in equation (3.4.3) we obtain:

$$2\pi \partial_\varphi E_\varphi + \frac{L_p}{R_0} \partial_\theta E_\varphi = L_p \dot{B}_r^A + \frac{r}{R_0} [L_p \cos \varphi \dot{B}_r^A + 2\pi \sin \varphi E_\varphi - 2\pi \cos \varphi \partial_\varphi E_\varphi] . \tag{3.4.8}$$

The homogeneous solution of (3.4.8) is zero [20]. For finding the particular solution we write E_φ as a power series in r: $E_\varphi = E_\varphi^{(0)} + r E_\varphi^{(1)} + r^2 E_\varphi^{(2)} + \cdots$. This gives:

$$2\pi \partial_\varphi E_\varphi^{(0)} + \frac{L_p}{R_0} \partial_\theta E_\varphi^{(0)} = L_p \dot{B}_r^A$$

and

$$2\pi \partial_\varphi E_\varphi^{(1)} + \frac{L_p}{R_0} \partial_\theta E_\varphi^{(1)} = \frac{L_p}{R_0} \cos \varphi \dot{B}_r^A + \frac{2\pi}{R_0} \sin \varphi E_\varphi^{(0)} - \frac{2\pi}{R_0} \cos \varphi \partial_\varphi E_\varphi^{(0)}$$

for $E_\varphi^{(0)}$ and $E_\varphi^{(1)}$ respectively. The solution is:

$$E_\varphi^{(0)} = \frac{L_p \dot{B}_z^A}{2\pi(1-k^2)} \left[\sin\varphi\sin\theta + k\cos\varphi\cos\theta\right]$$

and

$$E_\varphi^{(1)} = -\frac{\dot{B}_z^A}{2}\cos\theta - \frac{\dot{B}_z^A k(1+2k^2)}{(1-k^2)(4-k^2)}\sin 2\varphi\sin\theta$$

$$-\frac{\dot{B}_z^A k^2(5+k^2)}{2(1-k^2)(4-k^2)}\cos 2\varphi\cos\theta$$

with

$$k = \frac{L_p}{2\pi R_0} .$$

The higher order Fourier terms in φ appear because h_θ contains the term $r\cos\varphi$, see equation (3.4.2). For the other electric field terms and the currents the power series approach is equivalent.

Due to the shielding currents the maximal transport current at low losses (I_{max}) is for small k approximated by:

$$I_{max} = \pi R^2 \left[\eta j_c - 2\sigma_\perp |\dot{B}_z^A| \frac{L_p}{2\pi} \cdot \frac{1}{k^2}\right]. \qquad (3.4.9)$$

The maximum value of $|\dot{B}_z^A|$ for which the centre of the wire is unsaturated is given by:

$$|\dot{B}_z^A| < \frac{\pi\eta j_c k^2}{\sigma_\perp L_p} \quad \text{(for small } k\text{)} . \qquad (3.4.10)$$

Notice that for this value of $|\dot{B}_z^A|$, I_{max} is zero. Furthermore, the coupling losses per unit volume are given by:

$$\frac{P}{\text{Vol}} = \frac{\sigma_\perp \dot{B}_z^{A^2}}{2}\left(\frac{L_p}{2\pi}\right)^2 + \frac{\sigma_\perp \dot{B}_z^{A^2}}{4} \cdot \frac{a^2}{k^2} \quad \text{(for small } k\text{)} , \qquad (3.4.11)$$

where the first and second term are due to the perpendicular and parallel component of the applied field $\dot{B}_z^A$ respectively. The first term is half of the value arising in case the field is perpendicular over the whole length of the wire.

Another commonly used approach for calculating the field and currents in a toroidal configuration is as follows: consider a straight wire and apply a spatially periodic time dependent magnetic field. The torus problem can be approximated by a straight wire in a spatially dependent magnetic field for small values of k [20].

4. Numerical solutions

4.1. Introduction

In the previous section, where analytical solutions were calculated we had to idealize the problem significantly in order to be able to perform the calculations. In this section we

investigate aspects concerning numerical solutions. The reason for performing numerical calculations is threefold:

(1) to find bounds for the validity of the analytical approximations (for design purposes),
(2) to compare non-trivial analytical solutions with numerical data (checks on the solution methods),
(3) to be able to obtain results where no analytical calculations are possible, mainly due to the non-linear **E–j** relation. The most important cases that cannot be treated analytically are:

    (1) $R_f \neq 0$, this case will not be considered in this article, see [10],
    (2) time dependency/transient phenomena including saturation,
    (3) $I^A \neq 0$,
    (4) calculation of the exact form of boundaries between positive/negative/unsaturated regions.

These items will be considered in this section. We treat the basic ideas of the numerical model and present some specific numerical results. The comparison between numerical and analytical results is performed for parallel applied magnetic fields.

Even the largest supercomputers are not able to cope with general 4 dimensional space-time problems due to large cpu times and high storage requirements. Therefore in general we have to reduce the dimensions of the problem using symmetry arguments like rotational symmetry (φ-invariance) or z-invariance. Consequence is that some terms in the Maxwell equations are not present anymore. The number of unknowns and the cpu time are reduced considerably.

4.2. Numerical model

Three important aspects can be determined concerning the numerical model:

$*$) Grid using the method of grid staggering,
$*$) Boundary conditions,
$*$) Non-linear **E–j** relation.

We now investigate every aspect in more detail.

4.2.1. Grid staggering
When considering a convenient grid, use is made of the so-called staggered space grid. Maxwell's equations in integral form read:

$$\int_{\partial s} \mathbf{B} \cdot d\mathbf{l} = \iint_S \mu_0 \mathbf{j} \cdot \mathbf{e}_n \, dS \,,$$

$$\int_{\partial s} \mathbf{E} \cdot d\mathbf{l} = \iint_S -\dot{\mathbf{B}} \cdot \mathbf{e}_n \, dS \,. \tag{4.2.1.1}$$

These equations are discretized second-order accurate in time and space. For the time discretization mostly the three point backward method is used and for the space discretiza-

tion the midpoint rule is used. These discretizations can be implemented very conveniently on a staggered space grid. As an example we consider a two dimensional $r - \varphi$ grid given in Fig. 4.1. Recognize that $\nabla \cdot \mathbf{B}$ and $\nabla \times \mathbf{E}$ are calculated at the same position (solid curve in Fig. 4.1), as well as $\nabla \times \mathbf{B}$ and $\nabla \cdot \mathbf{j}$ (dashed curve). The formulae for discretizing the equations using the solid basic cell as considered in Fig. 4.1 read:

$$\nabla \cdot \mathbf{B} = 0: \quad (i + 1)\, \Delta\varphi\, B_r(i + 1, j) - (i - 1)\, \Delta\varphi\, B_r(i - 1, j)$$

$$+ B_\varphi(i, j + 1) - B_\varphi(i, j - 1) = 0 ,$$

$$(\nabla \times \mathbf{E})_z = -\dot{B}_z: \quad (i + 1)\, \Delta\varphi\, E_\varphi(i + 1, j, k) - (i - 1)\, \Delta\varphi\, E_\varphi(i - 1, j, k) + E_r(i, j - 1, k)$$

$$- E_r(i, j + 1, k) = -2i\, \Delta r\, \Delta\varphi\, \dot{B}_z(i, j, k) ,$$

with

$$\dot{B}_z(i, j, k) = (3 B_z(i, j, k) - 4 B_z(i, j, k - 1) + B_z(i, j, k - 2))/(2\, \Delta t) .$$

The indices i, j, k are related to the r, φ, t coordinates, respectively. The discretization of the equations using the dashed basic cell are similar to the above given discretizations.

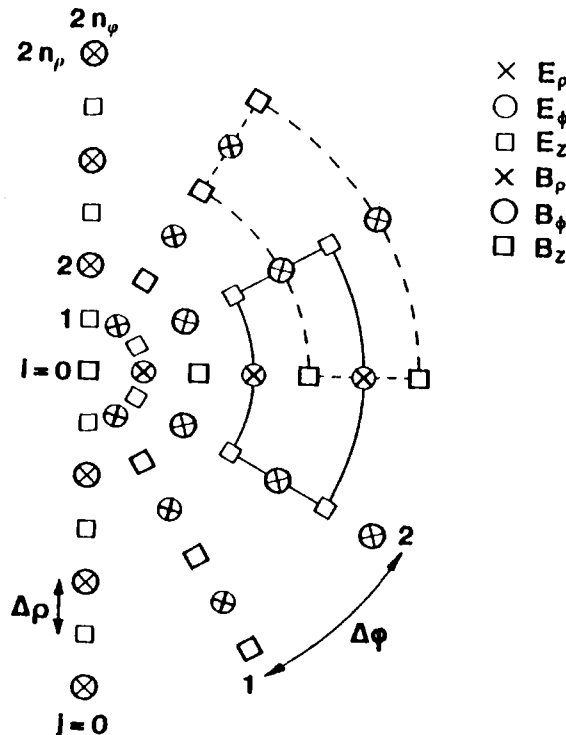The basic molecules in three dimensions for both equations are given in Fig. 4.2,

Fig. 4.1. A small version of the grid, used for the discretization of the electromagnetic field inside the wire $(n_\rho = 2, n_\phi = 3)$ [5].
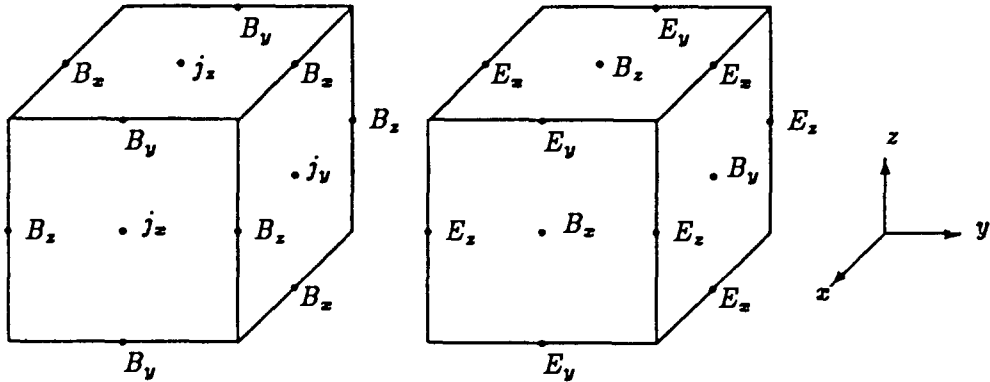
Fig. 4.2. The two basic molecules for the 3-D staggered grid [10].

respectively [10]. These two molecules can be combined to a staggered 3D grid (Fig. 4.3). Notice that the staggering of these two molecules is imposed by the coupling of the two sets of Maxwell's equations. This grid, useful for isotropic and weak anisotropic media, can also be used for superconducting media. For practical superconducting wires with twistlength very large compared to the radius, the superconducting constitutive equation is merely a relation between the axial component of the electric field and the current density. One has to make an interpolation of the axial component of the electric field for calculating the superconducting current density in the other direction. This interpolation is a weak point of the numerical method because it influences the iteration process, which will be described later. Normally this interpolation can be circumvented for a 2D grid, by adapting the grid. The numerical scheme is second order consistent at those points where **E** and **B** are sufficiently smooth. At the free boundaries, however, the consistency is only first order in the discretization steps, because then j_φ and j_z are not continuously differentiable functions of **E**. Furthermore, there is a limitation on the time step because the initial guess (due to the iteration process, treated in Section 4.2.3) may be too inaccurate for large time steps [5].

4.2.2. Boundary conditions

The boundary condition for the currents is $j_r(R) = 0$ which can easily be implemented on the grid.
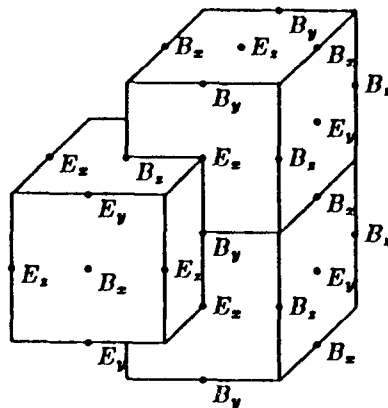

Fig. 4.3. The three dimensional staggered grid for the computation of the electromagnetic fields [10].

In general, for solving Maxwell's equations, the magnetic field in all space must be considered: so not only in the interior of the wire but also in the vacuum surrounding it or even in the centre for a hollow wire. The boundary condition is formulated for $r \to \infty$ where the induced magnetic field must vanish. However, we are only interested in the solution in the interior of the wire and need boundary conditions on $r = R$. They can be found considering that outside the wire the magnetic field satisfies $\Delta \mathbf{B} = 0$ because no currents are present. The magnetic field components outside the wire can be written using double summations in φ and z over an infinite number of terms which then are matched to the magnetic field at the surface of the wire itself. In this way the boundary condition for $r \to \infty$ is translated into a boundary condition at $r = R$. Result is that we only have to discretize the equations in the interior of the wire with correct boundary conditions at $r = R$ and $r = 0$.

This translation of the boundary condition will now be explained in detail for a z-invariant $r - \varphi$ grid (Section 4.2.2.1) and a φ-invariant $r - z$ grid (Section 4.2.2.2) where only one summation in the Laplacian solution remains.

4.2.2.1. Boundary condition at $r = R$ for the magnetic field for a z-invariant problem
For a uniform applied magnetic field in the y-direction perpendicular to an infinitely long circular wire (so $B_z(R) = 0$) we can match B_r and B_φ at $r = R$ with the $r - \varphi$ dependent Laplacian solution outside the wire ($r \geq R$) (see Section 2.4):

$$B_r(r, \varphi) = B_y^A(t) \sin \varphi + \sum_{n=1}^{\infty} a_n \left(\frac{R}{r}\right)^{n+1} \sin n\varphi \,,$$

$$B_\varphi(r, \varphi) = B_y^A(t) \cos \varphi + \sum_{n=0}^{\infty} - a_n \left(\frac{R}{r}\right)^{n+1} \cos n\varphi \,.$$

$$(4.2.2.1.1)$$

Here use is made of the symmetry arguments $A_r(r, \varphi - \tfrac{1}{2}\pi) = -A_r(r, \tfrac{1}{2}\pi - \varphi)$ and $A_\varphi(r, \varphi - \tfrac{1}{2}\pi) = A_\varphi(r, \tfrac{1}{2}\pi - \varphi)$ with A_r, A_φ the r and φ components of any vector field $\mathbf{A}$. The terms a_n can be eliminated using the orthogonality of $\sin n\varphi$ and $\cos n\varphi$. This provides a relation between B_r and B_φ, which at the wire surface $r = R$ gives:

$$\int_0^\pi B_\varphi(R) \, d\varphi = \frac{\mu_0 I^A(t)}{2R} \quad \text{(for } n = 0\text{)} \,,$$

$$\int_0^\pi B_\varphi(R, \varphi) \cos n\varphi \, d\varphi + \int_0^\pi B_r(R, \varphi) \sin n\varphi \, d\varphi = \pi B_y^A(t) \delta_{1,n} \quad \text{(for } n \geq 1\text{)} \,.$$

Here $\delta_{i,j}$ is the Kronecker delta. For the numerical grid refer to Fig. 4.1. With $\Delta\varphi = \pi/N_\varphi$ for any $(N_\varphi + 1)$ equally spaced B_φ points on the wire surface ($r = R$), this relation can be used N_φ times in its discretized form:

$$\sum_{j=1}^{N_\varphi + 1} B_\varphi(R, \varphi_j) \cos n\varphi_j + \sum_{j=1}^{N_\varphi} B_r'(R, \varphi_j) \sin n\varphi_j = \Delta\varphi \quad (n = 1, N_\varphi)$$

and the symbol B_r' is introduced, because in our grid B_r is not defined at the surface, but at positions half a cell dimension inside the wire. To calculate B_r' it is approximated by a linear interpolation of the value $B_r(\varphi_j)$ at a grid point near the surface and $B_r''(\varphi_j)$ at an imaginary point half a cel dimension outside the wire. Using the Maxwell equation $\nabla \cdot \mathbf{B} = 0$ at the wire

surface, the boundary equations for B_φ are found. The $(N_\varphi + 1)^{\text{th}}$ equation for $B_\varphi(R, N_\varphi + 1)$ is

$$\sum_{j=1}^{N_\varphi + 1} B_\varphi(R, j) = \frac{\mu_0 I^{\text{A}}(t)}{2R\,\Delta\varphi} .$$

4.2.2.2. Boundary conditions at $r = R$ for the magnetic field for a φ-invariant problem

Consider an infinitely long circular wire in a periodic applied magnetic field with periodicity length L_z with only r and z components. This φ-invariant problem will be discussed in more detail in Section 4.3.2B. We match B_r and B_z at $r = R$ with the $r - z$ dependent Laplacian solution outside the wire $(r \geq R)$ where use is made of the symmetry argument $\partial_z B_z = 0$ at $z = 0$:

$$B_z(r, z) = B^{\text{A}}(t)I_0(pr)\cos pz + \sum_{n=1}^{\infty} - a_n K_0(npr)\cos npz ,$$

$$B_r(r, z) = B^{\text{A}}(t)I_1(pr)\sin pz + \sum_{n=1}^{\infty} a_n K_1(npr)\sin npz . \tag{4.2.2.2.1}$$

Elimination of a_n gives, substituting $r = R$:

$$K_1(npR)\int_0^{L_z} B_z(R)\cos npz\,\mathrm{d}z + K_0(npR)\int_0^{L_z} B_r(R)\sin npz\,\mathrm{d}z = \frac{L_z}{2} B^{\text{A}}(t)\delta_{1,n}\frac{L_z}{2\pi R}$$

using the Wronskian [21]: $I_\nu(z)K_{\nu+1}(z) + I_{\nu+1}(z)K_\nu(z) = 1/z$. Using the symmetry condition we see that $\int_0^{L_z} = 4\int_0^{L_z/4}$, so only the interval $0 \leq z \leq L_z/4$ must be calculated. The numerical implementation is similar to the $r - \varphi$ grid (Section 4.2.2.1).

4.2.3. Non-linear E–j relation

Due to the non-linearity in the E–j relation the numerical solution cannot be found directly but the problem is linearized and iterated.

The iteration process [5, 10] is fully based on the non-linear relation between the parallel component of the electric field $E_\parallel$ and the superconducting current density j_p. The iteration process is as follows: every grid point is labelled. A grid point is labelled to be positively saturated if the previous or initial value of $E_\parallel > 0$, negatively saturated if $E_\parallel < 0$ and unsaturated otherwise. We use the constitutive equations related to the labelling and solve the set of equations. With the solution we check the predicted $E_\parallel$. If the prediction is not equal to the solution we change the label, but for convergence reasons one should not allow an element to change from a negatively saturated element into a positively saturated one or vice versa, but only allow saturated elements to turn into unsaturated ones or vice versa. There is no mathematical proof that this iteration scheme converges but in practice it works very well. Because $E_\parallel$ is calculated using E_φ and E_z it is best to calculate both electric field components at the same position.

4.3. Numerical results

In this section we present numerical results. The most general grid is 4 dimensional in space-time but due to symmetry arguments the time dependency can be included or not and

the space grid can be 1, 2 or 3 dimensional. Subsection 4.3.1 deals with DC and stationary problems and in subsection 4.3.2 non-stationary problems are considered. In each subsection the dimension of the space grid is used to classify the results. Furthermore we compare some numerical and analytical results, mainly in case of parallel applied magnetic fields.

When not specifically mentioned, we consider a circular multifilamentary twisted wire.

4.3.1. DC and stationary problems

The dimension of the space grid is used to classify the results:

(A) 2-dimensional space grid

An infinitely long multifilamentary wire carrying a DC transport current in a constant perpendicular applied magnetic field [22]. The set of equations is: $\nabla \times \mathbf{B} = \mu_0 \mathbf{j}$; $\nabla \times \mathbf{E} = \mathbf{0}$. The problem is z-invariant so we need a 2D grid in the $r - \varphi$ coordinates. We have to translate the boundary conditions for $\mathbf{B}$ at $r \to \infty$ to a condition for $\mathbf{B}$ at $r = R$ as was already explained (Section 4.2.2.1). The non-linear $\mathbf{E}$–$\mathbf{j}$ relation (2.2.7) is used, with $j_c(B_\perp)$ given by the Kim relation [23] and $E_0^{DC} = 0$. Zero, one or two boundaries separating saturated regions can appear. The mesh contains about 10×10 grid points on the $r - \varphi$ surface given by $0 \leqslant r \leqslant R$ and $0 \leqslant \varphi \leqslant \pi$. In Fig. 4.4 the saturated and non saturated regions are given in case 2 boundaries appear. In Figs 4.5 and 4.6 the $E_z - I_z$ relation for the whole wire is given at constant applied field $B^A = 2T$ and at constant twistpitch $L_p/R_w = 20$ respectively. As can be seen, there is a very large increase in E_z as saturation occurs.

Another DC problem is described by Boschman [24] where he calculates the solution for superconducting films connected through matrix material. J_c of every film is a periodic function of x: $J_{c,1}(x) = J_0(1 - 2|x|/L)$ and $J_{c,2}(x) = J_0 - J_{c,1}(x)$ with total critical current J_0. For this z-invariant problem we need a 2D xy grid. For 2 values of I^A the saturation pattern is shown in Fig. 4.7. This current transfer through the matrix material between the filaments causes Ohmic losses.

In this class of problems we can also consider the stationary solution (i.e. $\dot{\mathbf{B}}^I = \mathbf{0}$) for an infinitely long wire subject to a perpendicular AC magnetic field, constantly increasing in time. The only difference with the already treated problem is the modified
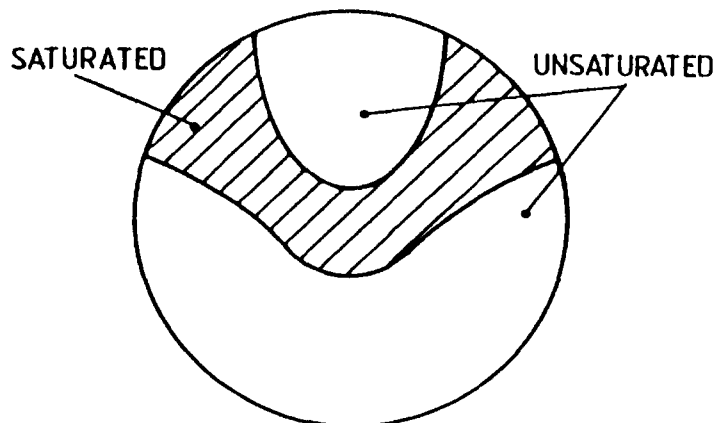

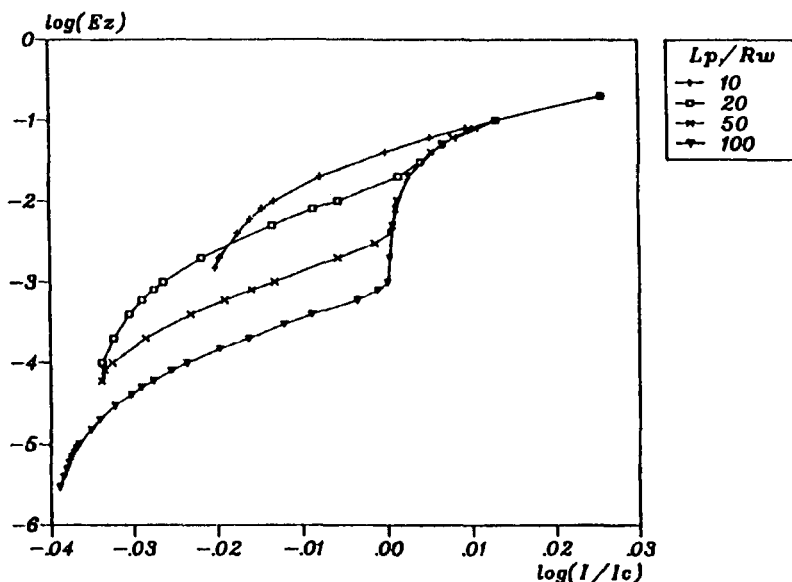*Fig. 4.4.* Occurrence of saturated and unsaturated regions in the wire when two boundaries are present [22].

Fig. 4.5. Electric field as a function of the scaled current, for various values of L_p/R_w at an applied field of 2 tesla [22].

equation: $\nabla \times \mathbf{E} = -\dot{\mathbf{B}}^A$. The saturation boundaries for zero applied current are given in Fig. 4.8 [10]. Region 3 is saturated by coupling currents and cannot contribute to the transport current. Only region 1 can carry transport current which means that the maximum transport current I_{max} for a perpendicular field rate is reduced as described by [10]:

$$I_{max} = I_c\left[1 - \frac{\sigma_\perp R|\dot{\mathbf{B}}_\perp|}{\eta j_c} \cdot \frac{1}{\beta^2 R^2}\right].$$
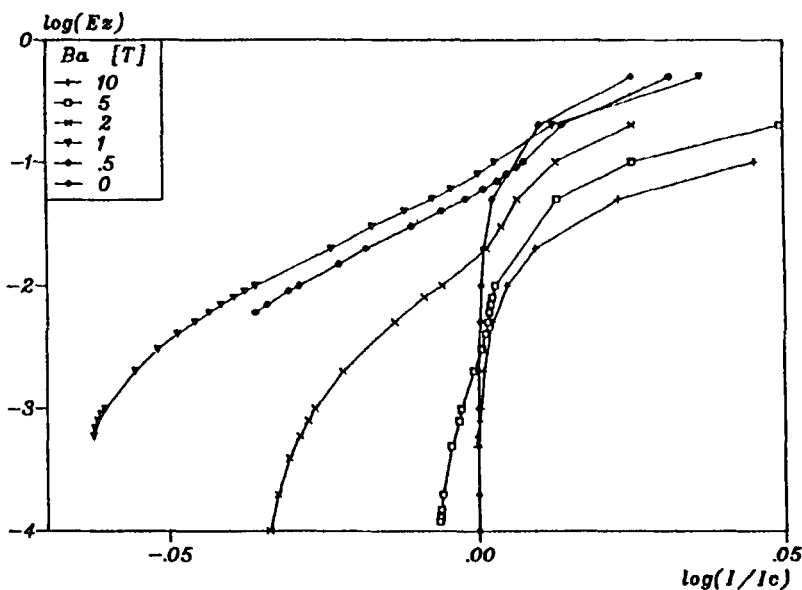
$$(4.3.1.1)$$

Fig. 4.6. Electric field as a function of the scaled current, for various values of the applied field, and $L_p/R_w = 20$ [22].
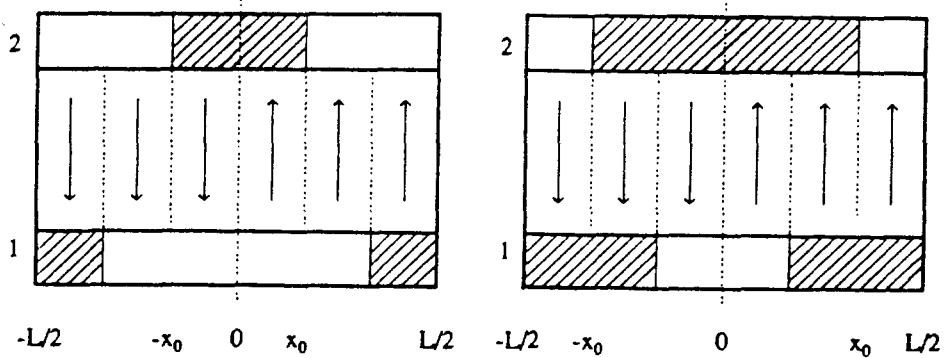
Fig. 4.7. Saturated (shaded) and unsaturated regions of the superconducting surface layers. The arrows indicate the direction of the current transfer between the layers [24].

The $r - \varphi$ grid size is about 18×42 in the $r - \varphi$ surface given by $0 \leqslant r \leqslant R$ and $0 \leqslant \varphi \leqslant 2\pi$.

(B) 3-dimensional space grid

An infinitely long multifilamentary wire carrying a DC transport current with no applied field. The wire properties are not constant, but a periodic function of the axial coordinate z. For the i-th superconducting filament we consider e.g.:

$$j_{c_i}(z) = j_c \left[1 + \alpha_i \sin\left(\frac{2\pi z}{L_z} + \varphi_i\right) \right] ,$$ (4.3.1.2)

with $0 \leqslant \alpha_i \leqslant 1$, L_z the periodicity length and φ_i some phase. This problem cannot be calculated analytically using Fourier expansions because of the non-linearity in the **E**–**j** relation.

The set of equations is: $\nabla \times \mathbf{E} = \mathbf{0}$ and $\nabla \cdot \mathbf{j} = 0$. A 3D x, y, z-grid is used taking into account one period length L_z. These calculations are performed investigating the influence of non-uniformity of wire properties on n values as described by equation (2.2.3).
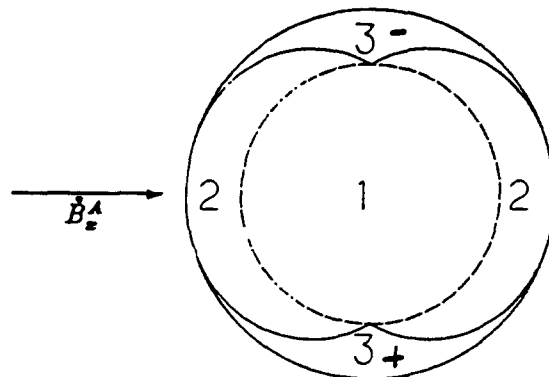

Fig. 4.8. The three different regions for the current distribution of a wire in an applied field $\dot{B}_x^A$. Regions 1 and 2 are unsaturated, region 3 is saturated [10].

4.3.2. Non-stationary problems

Here also the dimension of the space grid is used to classify the results:

(A) 2-dimensional space-time grid

An infinitely long circular wire in an AC magnetic field parallel to the z-axis. The set of equations is: $\nabla \times \mathbf{B} = \mu_0 \mathbf{j}$; $\nabla \times \mathbf{E} = -\dot{\mathbf{B}}$. Furthermore the non-linear $\mathbf{E}$–$\mathbf{j}$ relation (2.2.7) is used. For this $\varphi - z$-invariant problem the boundary conditions are:

$$E_\varphi(r = 0, t) = 0, \qquad B_\varphi(r = 0, t) = 0, \qquad B_\varphi(r = R, t) = \frac{\mu_0 I^A(t)}{2\pi R}, \quad \text{and}$$

$$B_z(r = R, t) = B_z^A(t).$$

The initial conditions are $\mathbf{E} = \mathbf{B} = 0$ for $t \leqslant 0$. Using Maxwell's equations we directly obtain: $E_r = B_r = 0$ and so we have to solve 5 unknowns: E_φ, E_z, j_s, B_φ, B_z using the remaining 4 Maxwell's equations and constitutive equation (2.2.7). Notice that in the unsaturated regions where $E_\| = 0$ the relation $\dot{B}_\varphi = \beta r \dot{B}_z$ holds. Starting from the virgin state, we see that $B_\varphi = \beta r B_z$ until saturation occurs.

Concerning the constitutive equations E_φ, E_z and j_s should be calculated at the same position. The magnetic field components should be calculated in between. Because 3 of the 4 boundary conditions are given in terms of the magnetic field, it is most convenient to calculate the magnetic field components at $r = 0$ and $r = R$. Then we only have to calculate E_φ ($r = 0$) using an extrapolation of the internal E_φ values. The grid we arrive at is given in Fig. 4.9.

In the previous section an analytical approximation for the maximum amplitude not saturating the interior of the wire and the loss power were given under the assumption that all return current flows in a surface shell. Numerical approaches to the problem show that some peculiar and unexpected effects are, however, present. Figure 4.10 shows the time development of the saturated regions when a z-invariant $B_z^A = \sin(\omega t)$ is applied at $t = 0$, furthermore $I^A = 0$. When $\omega t < \pi/2$ a negative saturated region starts in the outer region of the wire. At $\omega t = \pi/2$ a positive saturated region starts at $r = R$ but the negative saturated region moves inward and disappears at $\omega t = 3\pi/2$. This pattern repeats each period. In Fig. 4.11 a small time independent transport current is present and, as can be seen, the positive saturated regions penetrate much further than the negative ones. This means that a parallel applied field in an unexpected way reduces
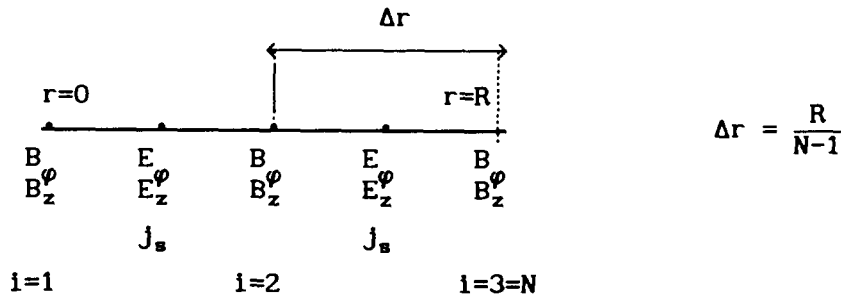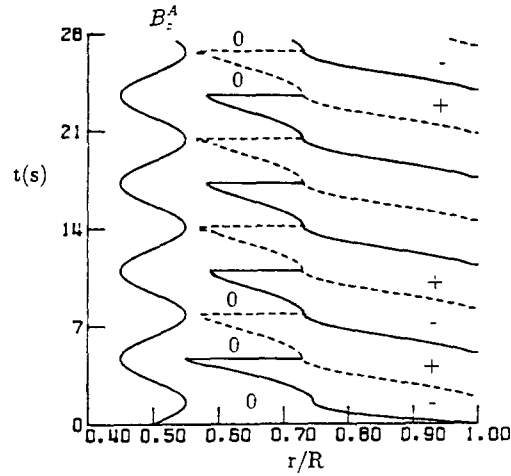

Fig. 4.9. Grid for case 4.3.2A.

Fig. 4.10. Numerical solution of the saturation of the filaments for a uniform B_z^A with sinusoidal time dependence and no transport current.
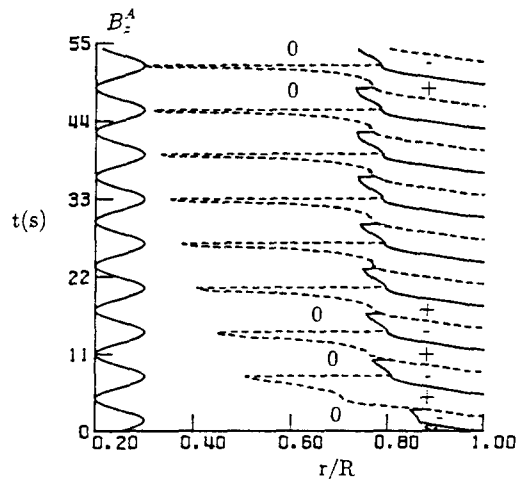
the current carrying capacity of the wire since at the outside a double layer of positive and negative saturated current exists. When we apply a sinusoidal magnetic field:

$$B_z^A(t) = B_0 \sin \omega t = \frac{B_0}{2i} (e^{i\omega t} - e^{-i\omega t}) \tag{4.3.2.1}$$

the response of the electric field is (see Section 3.3):

$$E_\varphi(t) = - \frac{\omega}{2} (g\, e^{-i\omega t} + g^*\, e^{i\omega t}) . \tag{4.3.2.2}$$

Notice that both B_z^A and E_φ are real functions of time. Furthermore there is no applied

Fig. 4.11. Numerical solution of the saturation of the filaments for a uniform B_z^A with sinusoidal time dependence with a transport current of about 0.2 of the critical current.

current so $B_\varphi(R) = 0$. Calculating the mean loss per unit length ($\bar{P}$) using Poynting's theorem we get:

$$\bar{P} = - \frac{\omega}{2\pi} \int_0^{2\pi} \int_0^{2\pi/\omega} \frac{1}{\mu_0} (E_\varphi(R)B_z^{A*}(R) - E_z(R)B_\varphi^*(R))R \, \mathrm{d}\phi \, \mathrm{d}t \left[\frac{W}{m} \right]. \qquad (4.3.2.3)$$

Using the analytical approach from Section 3.3 we obtain:

$$\bar{P} = - \frac{2\pi R}{\mu_0} \omega \left(\frac{\mathrm{i}g(R) - \mathrm{i}g^*(R)}{4} \right) B_0 = - \frac{\pi R \omega B_0}{2\mu_0} (\mathrm{i}g(R) - \mathrm{i}g^*(R)),$$

$$(4.3.2.4)$$

$$\bar{P} = \frac{\pi R \omega B_0}{\mu_0} \cdot \mathrm{Im}(g(R)),$$

with Im the imaginary part of a complex number.

Only the imaginary part of $g(R)$ appears in the loss term. This is easy to see because for real values of $g(R)$ the phase difference between B_z^A and $E_\varphi(R)$ is $\pi/2$, resulting in no loss because of the orthogonality between the sine and cosine function. $\bar{P}$ can also be found by calculating the dissipation directly from **E** and **j**:

$$\bar{P} = \frac{\omega}{2\pi} \int_0^{2\pi/\omega} \int_0^R \int_0^{2\pi} \mathbf{E} \cdot \mathbf{j}r \, \mathrm{d}r \, \mathrm{d}\varphi \, \mathrm{d}t, \qquad (4.3.2.5)$$

with

$$\mathbf{E} \cdot \mathbf{j} = \sigma_\parallel E_\parallel^2 + \sigma_\perp E_\perp^2 + E_\parallel \eta j_p. \qquad (4.3.2.6)$$

Numerically we can calculate either the contour integral (equation (4.3.2.3)) or the surface integral (equation (4.3.2.5)). Despite the higher work load, the surface integral is calculated because:

(1) Using the contour integral we need $E_\varphi(R)$ which should be calculated *extrapolating* from interior values. Using equation (4.3.2.4) we see that the loss is very sensitive to the phase difference between $B_z(R)$ and $E_\varphi(R)$. Calculating $E_\varphi(R)$ by extrapolation, this phase difference is calculated very inaccurately.
(2) The time integration of the surface integral is a summation of only positive terms which is not the case for the time integration of the contour integral.

For this type of problem (sinusoidally applied uniform B_z field, no transport current) we now compare numerical and analytical results. In Fig. 4.12 the scaled loss $2\pi\bar{P}/(\omega^2 B_0^2)$ is given as function of the amplitude of the applied field B_0. The complete parameter setting is: $B_z^A = B_0 \sin t$; $I^A = 0$; $R = 10^{-3}$ m; $L_p = 0.1$ m; $R_f = 0$; $j_c = 10^9$ A/m^2; $\eta = 0.5$ and $\sigma = 10^9$ (Ωm)$^{-1}$. Grid parameters: $\Delta r = R/50$ and $\Delta t = 2\pi/200$. Also the analytically calculated loss term (see equation (4.3.2.4)) using the linearized set of equations (see Section 3.3) is indicated in the figure.

For small values of B_0 there is perfect agreement between the numerical and analytical results because on the numerical grid no saturation occurs, resulting in a linear problem. The only loss term that contributes to the total loss is $\sigma_\perp E_\perp^2$. The deviation which starts at $B_0 = B_1$ can be explained as follows: for $B_0 > B_1$ outer grid

cells saturate. The loss terms $\sigma_{\parallel} E_{\parallel}^2$ and $E_{\parallel} \eta j_p$ then also contribute to the total loss term. When saturation occurs the reason for deviation between numerical and analytical result is twofold:

(1) in general: the saturated shielding current is dissipative while in the analytical approximation the surface current is considered to be non-dissipative;

(2) for this specific situation: at the surface the positively and negatively saturated shielding currents do not cancel but both positively and negatively saturated regions appear next to each other, as was already mentioned. This increases the loss even more.

Notice that the first deviation between analytical and numerical results depends on the grid size Δr. When Δr decreases, saturation occurs at the outer grid cells for smaller values of B_0 so in the limit $\Delta r \to 0$ saturation occurs for $B_0 \to 0$.

For increasing amplitude B_0, the saturated regions penetrate more towards the centre of the wire. For $B_0 = B_2$ also a saturated region grows outward from the centre of the wire and the loss increases even more. The value of B_2 is $5T$ which follows from equation (3.3.5). For very large values of B_0 the term $E_{\parallel} \eta j_p$ can be neglected compared to the Ohmic loss terms. The linear behaviour is dominant and the deviation between numerical and analytical results decreases.

(B) 3-dimensional space-time grid

An infinitely long circular wire in an AC perpendicular magnetic field. The solution of the Maxwell equations for this z-invariant problem has been determined with boundary conditions $B_z^A(t) = 0$ and B_φ and B_r at $r = R$ using the previously mentioned series expansion, Section (4.2.2.1). All three components of $\mathbf{E}$ and $\mathbf{B}$ and the superconducting
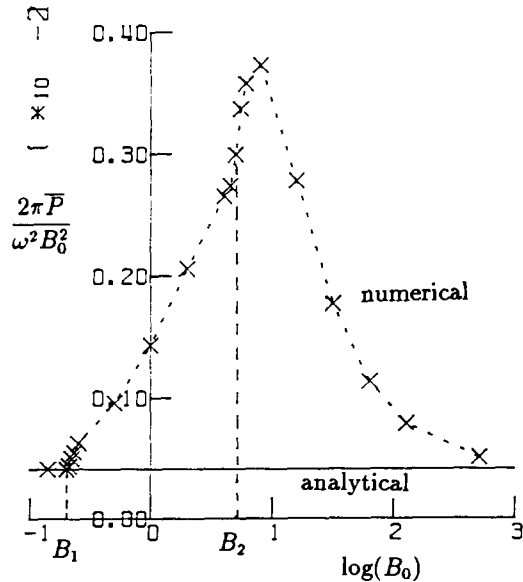

Fig. 4.12. $2\pi \bar{P}/(\omega^2 B_0^2)$ as function of $\log(B_0)$. The numerical and analytical results are indicated. For further explanation see text.

current density j_s must be calculated on an $r - \varphi - t$ grid. In Fig. 4.13 the degree of saturation is shown for 4 moments in time for an AC transport current in phase with a sinusoidal applied field [5].

In this class of problems we consider a second one. An infinitely long circular wire in a periodic applied magnetic field with periodicity length L_z:

$$(B_r^A, B_\varphi^A, B_z^A) = B^A(t)(I_1(pr) \sin pz, 0, I_0(pr) \cos pz) .$$

This problem is φ-invariant and periodic in z, resulting in an $r - z - t$ grid. We use the Maxwell equations with the boundary conditions:

(1) $B_\varphi(z, r = 0, t) = 0,$
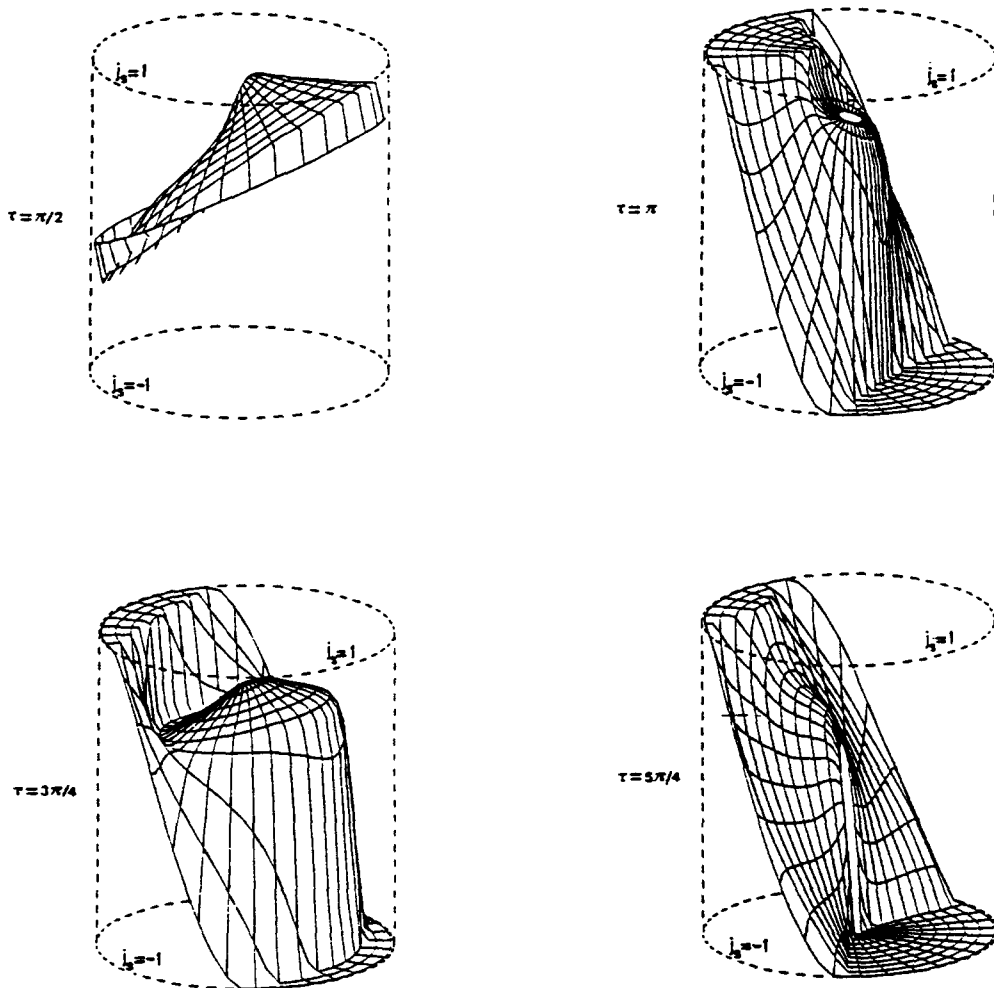(2) $B_\varphi(z, r = R, t) = 0$ (no applied current),

Fig. 4.13. The degree of saturation for 4 moments in time for an AC transport current in phase with a sinusoidal applied field [5].

(3) $E_\varphi(z, r = 0, t) = 0$,

(4) $B_\varphi(z, R)$ and $B_z(z, R)$ are calculated using series expansions, see Section 4.2.2.2. (Notice that in the z-inv. problem (case 4.3.2A) we had $B_z(R) = B_z^A$.)

(5) at $z = \frac{1}{4} L_z$: $E_\varphi = E_z = B_\varphi = B_z = j_s = 0$,

(6) at $z = 0$: $\partial_z E_\varphi = \partial_z E_z = \partial_z B_\varphi = \partial_z B_z = \partial_z j_s = 0$.

So we have a grid for $0 \leqslant z \leqslant \frac{1}{4} L_z$. Not all 7 unknowns have to be calculated because we can very easily eliminate E_r and B_r using:

$$E_r = - \frac{\partial_z B_\varphi}{\mu_0 \sigma_\perp}$$

and $\dot{B}_r = \partial_z E_\varphi$ resulting in the set:

$$\frac{\partial_{zz} B_\varphi}{\mu_0 \sigma_\perp} + \partial_r E_z = \dot{B}_\varphi \,,$$

$$\frac{1}{r} \partial_r r E_\varphi = -\dot{B}_z \,,$$

$$\partial_{zz} E_\varphi - \partial_r \dot{B}_z = \mu_0 \dot{j}_\varphi \,,$$

$$\frac{1}{r} \partial_r r B_\varphi = \mu_0 j_z \,,$$
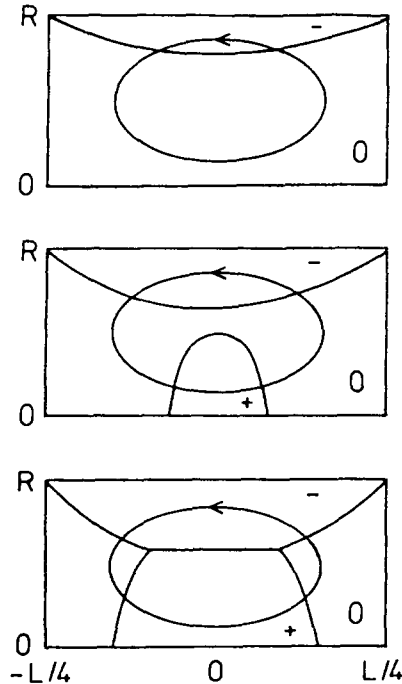
Fig. 4.14. The development of the saturated regions for periodic B_z^A and linear time dependence. For further explanation see text. The current pattern is indicated.

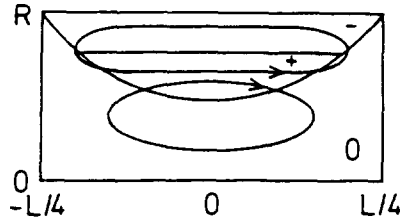*Fig. 4.15.* Momentary solution of saturated regions for periodic B_z^A with sinusoidal time dependence.

plus constitutive equation (2.2.7) for the 5 unknowns B_φ, B_z, E_φ, E_z and j_s. This reduction from 7 to 5 unknowns is not considered in the first problem of this class because the elimination is not easy due to the φ dependence. Figure 4.14 shows the development of the saturated regions for $B^A(t) = \alpha t$. The upper picture shows the boundary of the outside region for small t. The middle picture shows the start of the development of the inner saturated region at $B_z^A \sim \mu_0 \eta j_c L_p / 4\pi$ [16] whereas the lower picture shows the final state of the saturated regions for $t \to \infty$. In Fig. 4.15 a schematic picture is given for $B^A(t) = \sin t$ at some time. As in the uniform case in the outer region saturation in both directions coexists. The minimal mesh size is about 20×10 grid points on the $r - z$ surface given by $0 \leqslant r \leqslant R$ and $0 \leqslant z \leqslant L_z/4$. Furthermore in one periodic cycle in time the solution is calculated in 20 time steps.

The figures 4.10 and 4.15 as well as the analytical analysis of Section 3.3 and Fig. 4.14 show that the z-invariant problem is a well defined limiting case of the problem periodic in z. The calculations show that superconducting twisted wires subjected to parallel magnetic fields can carry much less transport current than earlier reported in the literature [17].

5. Concluding remarks

In this article a framework has been presented concerning analytical and numerical calculations of the electromagnetic properties of composite superconducting wires. The basic analytical and numerical tools, applied to characteristic types of problems are presented. Furthermore a synopsis has been given of specific numerical calculations which enable the calculation of more complicated problems. As reported, numerical calculations sometimes show peculiar and unexpected effects.

The numerical and analytical problems considered are idealized cases. Numerical calculations of general cases are not performed due to large cpu times and high storage requirements. However, the response of a system subjected to general applied magnetic fields is not necessarily a linear combination of the responses of idealized cases. To find bounds for the use of idealized solutions in general situations, some complicated problems should be considered in the future.

A careful comparison of the analytical and numerical results for in essence the same setting can give a very good insight of what the different methods are capable of. Some comparisons are already given in this article but it will be worthwhile to make more comparisons in the future.

All calculations are performed under isothermal conditions. Taking into account also the

heat balance equation with appropriate initial and boundary conditions, a more detailed description of the problem is obtained.

6. List of symbols

B, B_r, B_φ, B_z	= magnetic induction and its components
C, C_n	= constant
$\mathscr{D}$	= electric displacement
E, E_r, E_φ, E_z	= electric field and its components
I	= transport current
I_0, I_1	= Bessel functions of the second kind and order 0 or 1
K_0, K_1	= Bessel functions of the second kind and order 0 and 1
j, j_r, j_φ, j_z	= current density and its components
J_0, J_2	= Bessel functions of the first kind of order 0 and 2
j_s	= superconducting part of j_z
$J_\parallel, J_z, J_\varphi$	= components of the surface current
L	= half the length of the sample
L_z	= period length of the applied field
L_p	= twist length of the wire
M	= magnetization
n	= integer
N_f	= number of filaments
P	= $2\pi/L_z$
R	= radius of the wire
R_f	= filament radius
R_0	= mean radius of the torus
u	= $npr = 2n\pi r/L_z$
U	= $2\pi n R/L_z$
T	= temperature
α	= constant of functions of t only
β	= $2\pi/L_p$
η	= fraction of the superconductor
$\sigma_r, \sigma_\perp, \sigma_\parallel, \sigma_{\varphi\varphi}, \sigma_{\varphi z}, \sigma_{zz}$	= components of the conductivity tensor in the $r, \perp, \parallel$ or r, φ, z system
τ	= time constant
ψ	= twist angle, tg $\psi = \beta r$

Subscripts:

n, m	= mode number
r, φ, z, t	= components in cylindrical coordinate system and time
x, y, z	= components in cartesian coordinates

Superscripts:

A	= applied
I	= induced

Operators:

$\nabla \cdot$	= divergence
$\nabla \times$	= curl
$\cdot$	= time derivative
$'$	= derivate w.r.t. the argument
Im	= the imaginary part of a complex number.

References

1. J.D. Jackson, *Classical Electrodynamics*. Wiley and Sons, New York (1962).
2. W.J. Carr Jr., Electromagnetic theory for filamentary superconductors. *Phys. Rev.* B11 (1975) 1547–1554.
3. W.J. Carr, *AC Loss and Macroscopic Theory of Superconductors*. Gordon and Breach (1983).
4. K. Kanbara, Y. Kubota and T. Ogasawara, *Proc. ICEC* (1981) 715.
5. P.C. Rem, Numerical models for AC superconductors. Enschede: PhD Thesis, University of Twente (1986).
6. E.M.J. Niessen and L.J.M. van de Klundert, The effective transverse resistivity in multifilamentary conductors, to be published.
7. G.L. Dorofejev, A.B. Imenitov and E.Yu. Klimenko, Voltage-current characteristics of type III superconductors. *Cryogenics* 20 (1980) 307–312.
8. E.Yu. Klimenko and N.N. Martovetsky, Analyses of conductor behaviour in the superconducting toroidal magnet system of the tokamak T-15 installation. *Cryogenics* 27 (1987) 238–242.
9. A.P. Martinelli and B. Turck, Some effects of field orientation on the magnetization of superconducting wires. *Cryogenics* 18 (1978) 155–161.
10. R.A. Hartmann, A contribution to the understanding of AC losses in composite superconductors. Enschede: PhD Thesis, University of Twente (1989).
11. M.N. Wilson, *Superconducting Magnets*. Oxford University Press, New York (1983).

12. J.A. Eikelboom and L.J.M. van de Klundert, Hysteresis losses in hollow superconducting filaments and in a multifilament system. *Cryogenics* 31 (1991) 354–362.

13. J.A. Eikelboom, AC losses in prototype conductors for the NET toroidal field coils. Enschede: PhD Thesis, University of Twente (1991).

14. E.M.J. Niessen and L.J.M. van de Klundert, Superconducting multifilamentary wires in inhomogeneous perpendicular a.c. fields. In: *Proc. of the International Symposium on AC Superconductors*. Smolenice, CSFR (1991) ISBN 80-900506-0-3.

15. L.J.M. van de Klundert, New developments on calculating and measuring AC losses in composite superconductors. In *Proc. MT12*, Leningrad (1991) Paper DB01.

16. E.M.J. Niessen, A. Nijhuis, E.J. Oetsen and L.J.M. van de Klundert, Current degradation and coupling losses in ring shaped wires due to applied magnetic field changes. In: *Proc. MT12*, Leningrad (1991) Paper DB03.

17. B. Turck, Courants de circulation et pertes dans les composites supraconducteurs soumis a une induction longitudinal variable. *Revue de physique appliquée* (1976) 369.

18. G. Ries and K.P. Jüngst, Filament coupling in multifilamentary superconductors in pulsed longitudinal fields. *Cryogenics* 26 (1976) 143–146.

19. *Fusion Technology* 14 (1988) no. 1.

20. E.M.J. Niessen, L.J.M. van de Klundert, R.M.J. van Damme, F.P.H. van Beckum and P.J. Zandbergen. Coupling losses in superconducting, torus shaped wires due to applied magnetic field changes. Submitted to *Journal of Eng. Mathematics* (1992).

21. M. Abramowitz and 1.A. Stegun, *Handbook of Mathematical Functions with Formulas, Graphs and Mathematical tables*. New York: John Wiley & Sons (1972).

22. D. ter Avest, Properties of the superconductor in accelerator dipole magnets. Enschede: PhD Thesis, University of Twente (1991).

23. Y.B. Kim, C.F. Hempstead and A.R. Strnad, Critical persistent currents in hard superconductors. *Phys. Rev. Lett.* 9 (1962) 306–309.

24. H. Boschman, On the resistive transition of composite superconductors. Enschede: PhD Thesis, University of Twente (1991).